PHYSICAL REVIEW E **71**, 031914 (2005)

Simulations of transient membrane behavior in cells subjected to a high-intensity ultrashort electric pulse

Q. Hu, S. Viswanadham, and R. P. Joshi
Department of Electrical and Computer Engineering, Old Dominion University, Norfolk, Virginia 23529-0246, USA

K. H. Schoenbach
Center for Bio-Electrics, and Department of Electrical and Computer Engineering, Old Dominion University, Norfolk, Virginia 23529-0246, USA

S. J. Beebe and P. F. Blackmore
Center for Pediatric Research and Department of Physiology, Eastern Virginia Medical School, Norfolk, Virginia 23501, USA

(Received 4 November 2004; published 29 March 2005)

A molecular dynamics (MD) scheme is combined with a distributed circuit model for a self-consistent analysis of the transient membrane response for cells subjected to an ultrashort (nanosecond) high-intensity ($\sim$0.01-V/nm spatially averaged field) voltage pulse. The dynamical, stochastic, many-body aspects are treated at the molecular level by resorting to a course-grained representation of the membrane lipid molecules. Coupling the Smoluchowski equation to the distributed electrical model for current flow provides the time-dependent transmembrane fields for the MD simulations. A good match between the simulation results and available experimental data is obtained. Predictions include pore formation times of about 5–6 ns. It is also shown that the pore formation process would tend to begin from the anodic side of an electrically stressed membrane. Furthermore, the present simulations demonstrate that ions could facilitate pore formation. This could be of practical importance and have direct relevance to the recent observations of calcium release from the endoplasmic reticulum in cells subjected to such ultrashort, high-intensity pulses.

DOI: 10.1103/PhysRevE.71.031914 PACS number(s): 87.16.Ac, 87.50.Rr, 87.50.−a, 87.17.Aa

I. INTRODUCTION

The use of very high electric fields (~ 0.01 V/nm or higher) with pulse durations in the nanosecond range [1–3] has been a very recent development in bioelectrics. Traditionally, most electroporation studies have focused on relatively low external electric fields (less than a kilovolt per centimeter), applied over time periods ranging from several tens of microseconds to milliseconds [4]. There appear to be inherent advantages in using short electric pulses. These include: (i) Negligible thermal heating, (ii) the ability to develop large electric fields and peak powers, with a lower energy input, (iii) the possibility of selecting the desired time scales (and frequency components) through pulse-width manipulation, and (iv) the ability to create large transmembrane potentials across subcellular organelles. This can effectively open the way to intracellular electromanipulation, without destroying the outer membrane [5].

Recent work on high-intensity, pulsed electric fields has led to the following significant observations [5–9]: (i) It is possible to maintain the integrity of the outer cell membrane despite the high (~ 0.02 V/nm average) electric fields. (ii) Multiple pulses have been observed to do more irreversible damage than single-shot electric shocks. (iii) Irreversible cell damage is seen to occur at the intracellular organelles (e.g., mitochondria), while the outer membranes remain intact [5]. (iv) Calcium is released from the intracellular endoplasmic reticulum in response to external voltage pulses [5–7]. (v) Cell apoptosis has been observed [5,8] for cells subjected to the short electrical pulses. Apoptosis in such *in vitro* experiments is defined by the presence of several well-defined markers, such as annexin-V binding, caspase activation, a decrease in forward light-scattering during flow cytometry, and of cytochrome c release into the cytoplasm. (vi) The observed apoptotic behavior appears to depend on the pulse duration. Thus, for cells subjected to external electric fields at a constant energy level, much stronger apoptosis markers were observed only for the longer ($\sim$300 ns) pulses, less at the shorter ($\sim$60 ns) durations, and almost negligible effects for a short 10-ns pulse of the same input energy. (vii) Externalization of phosphatidylserine (PS) occurs in response to a nanosecond pulse for average electric fields above 2 MV/m [10]. PS is an acidic phospholipid that is normally located on the inner leaflet of the lipid bilayer. In the presence of a strong external electric field, PS can be flipped to the outer leaflet of the membrane, marking the cell for macrophage scavenging.

The phenomena of intracellular calcium release in response to a high-intensity, nanosecond-time voltage pulse is a very recent observation [7,11,12], and the mechanism is not well understood. For example, Vernier *et al.* [7] used 30-ns, 2.5-MV/m pulses on human Jurkat T lymphocytes, and reported a marked intensification of calcium green fluorescence within seconds of pulse exposure. This indicated an increase in the intracellular calcium ion concentration, and the calcium burst was uniform across the cell. Beebe *et al.* reported on the electric pulse induced calcium mobilization from intracellular stores within the endoplasmic reticulum of HL-60 cells [11,12]. This was followed by calcium entry through the plasma membrane, possibly via store-operated channels [12]. Their experiments supported the hypothesis that high field pulses have effects that are largely independent of actions on the plasma membrane, and modulate intracellular signal mechanisms. In both sets of experiments, calcium release was an important consequence of voltage pulsing, and indicative of inducing specific cellular communication in a controlled manner through external means. Since calcium is involved in biochemical stimulation of molecular signaling pathways that lead to apoptosis, the use of such electrical pulses for selective cell killing becomes an interesting and distinct possibility.

An important goal of this contribution is to quantitatively model and understand some of the high field effects on biological membranes on the nanosecond time scale. In particular, the pore formation process, and possible ionic transport (either via nanopores or through the biomembrane structure), is of interest. Calcium ions seem to be important as has been noted in recent experiments and for their role in cell signaling. A possible explanation of calcium release from the intracellular stores might be the nanopore formation at the endoplasmic reticulum (ER). This contribution attempts to examine this aspect. In addition, the pore formation dynamics is probed, and the predictions of pore formation times in Jurkat cells shown to compare very well with available experimental data.

II. MODELING DETAILS

In this section, some relevant modeling details are provided. First, the molecular dynamics simulation scheme is discussed, and then calculations of the time dependent transmembrane voltage for self-consistent electrostatics are provided. The latter is based on a distributed electrical circuit model of a cell.

A. Molecular dynamics simulations

The molecular dynamics (MD) scheme was used to probe the electric-field induced effects on a typical membrane and on time-dependent ionic transport. The microscopic MD simulation approach is superior to continuum approaches. Advantages include: (i) inclusion of the collective, many-body interaction potentials at the nanoscale level; (ii) dynamical screening; (iii) avoidance of "mean-field" approximations; (iv) a natural inclusion of noise and statistical fluctuations; (v) self-consistent and dynamical transport calculations without arbitrary fitting parameters; and (vi) easy incorporation of arbitrary defects and nonuniformities, as well as complex geometries.

Veneble *et al.* [13] and Egberts *et al.* [14] applied this technique to dipalmitoyl-phosphatidyl-choline (DPPC) bilayers. Various other studies of lipid bilayer systems have since been reported [15–18] based on this numerical approach. MD simulations rely on the application of classical Newtonian mechanics for the dynamical movement of ions and neutral atoms, taking account of the many-body interactions within a realistic molecular representation of the biosystem [19–22]. Thus, for example, a segment of the lipid bilayer membrane or a channel protein is first constructed taking account of the initial geometric arrangement of all the atoms and their bonding angles. Regions of water containing user-specified ion densities are then defined on either side of the membrane to form the total simulation space. The most commonly used water models in water-lipid systems are the simple point charge (SPC) [22] and the extended simple point charge (SPCE) [23,24] representations. The SPCE yields better bulk properties (such as density, radial distribution functions, and dielectric constant) than the SPC model, which makes it a logical choice in molecular dynamics studies of bulk water. However, SPC has a better chemical potential in mixed systems, which makes it a better choice in studies of interfaces [18,25]. Additionally, in a bilayer system with enough water, a lack of screening of the lipid dipoles does not require the SPCE approach. Hence here the SPC model has been used.

Initial velocities, temperature, and pressure are set for all particles. In order to prevent the system energies from increasing with time due to the dynamic acceleration, velocities are typically rescaled periodically by coupling the system to a constant temperature bath [26]. Interactions between atoms are divided into nonbonded interactions, and bonded interactions between atoms connected by chemical bonds. For nonbonded interactions, partial charges and parameters for repulsion and attraction are assigned to each atom. The bonded interactions consist of bonds, angles, and dihedral terms. The bonds and angles are usually described as harmonic oscillators and dihedral angles are described by a suitable cosine expansion. A typical potential function is the truncated and shifted Lennard-Jones potential by which two particles mutually interact. The time step of the algorithm has to be carefully chosen to ensure the stability in integrating the equations of motion. Variations of the original Verlet algorithm [27], such as the leap-frog scheme [28], with time steps of about 1 fs are typically used, and the biggest time step reported have been about 50 fs.

In our study, the Groningen machine for chemical simulation (GROMACS) package [29–31] was used for the MD simulations of field-induced membrane effects, and VMD provided for visualization of the results. Details of the dipalmitoyl-phosphatidyl-choline (DPPC) force field for membrane molecular motion can be found elsewhere [32]. The system was coupled to a semi-isotropic pressure coupling of 1 atmosphere with compressibility of 4×10^{-5} along the x and y directions, and zero along the z direction. A heat bath of 323 K was chosen to retain the liquid phase of the membrane [33]. This value is slightly above the physiological temperatures of mammalian cells, and was chosen for the following reasons. (i) This temperature is above the phase transition temperature for DPPC. For realistic simulations, one needs to look at a fully hydrated, biologically relevant, fluid phase. (ii) This temperature has been used in experiments on DPPC, and data are available at 323 K [34,35]. (iii) This value is also in line with several simulation reports in the literature (e.g., Refs. [18,33,36]). (iv) Finally, the principle goal here is to focus on the electrically induced bioresponse. The nanopore formation over these short time scales is solely driven by the electric field. Temperature plays an insignificant role in poration, and no biochemical reactions are in play.

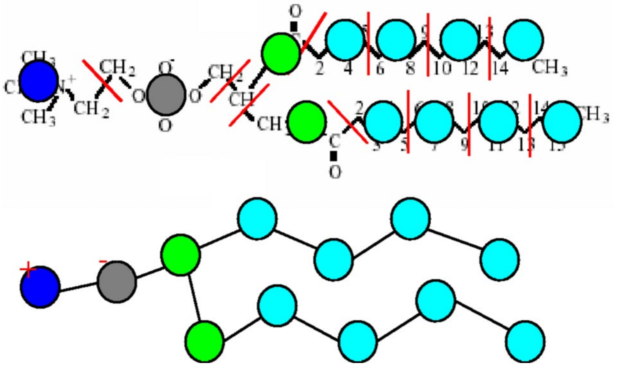

FIG. 1. (Color online) The dipalmitoyl-phosphatidyl-choline (DPPC) lipid molecule. (a) All atom representation, and (b) the coarse-grained model used.

Velocities of water and membrane molecules were generated subjected to Maxwellian distribution and were scaled with a coupling constant of 0.1 ps. The algorithms for pressure and temperature control were those discussed by Allen and Tildesly [19]. A 4-fs time step was used with constraints on the bond lengths within the lipids and on the water geometry. A twin cutoff scheme was employed for the nonbonded interactions with the cut-off radius of 0.9 nm for both the Lennard-Jones and the van der Waals interaction calculation. Particle-mesh Ewald (PME) summation was applied for calculations of the long range electrostatic interactions. The SPC water model was used with a simple point charge of $-0.82e$ on the oxygen atom, and charges of $0.41e$ on each of the hydrogen atoms. The O-H bond length was taken to be 0.1 nm with a $109°28'$ angle for the H-O-H bond. Both the bond length and bond angle for water are constrained by the SHAKE method [37,38]. All ions were treated as single Lennard-Jones centers, with the parameters for energy (ϵ_{ij}) and distance (σ_{ij}) taken from published literature [20,29,30]. Ions always have hydrated structure in water and the effective charge for solvated Na^+ is 0.7 and 1.4 for solvated Ca^{2+}. Periodic boundaries were applied, and the simulations carried out under constant pressure conditions. This method [26] allows the simulation box size to change so that the internal virial matches the external pressure.

The cell membrane was taken to comprise of DPPC lipid molecules. These are complex chain containing a large number of atoms, with a prominent "head" and two "tails" as shown in Fig. 1(a). In order to ease the computational burden and facilitate calculations in a reasonable amount of time, the complete DPPC molecule was reduced to a coarse grained model as shown in Fig. 1(b). Thus the choline, phosphate, glycerol, and methyl groups within DPPC were each aggregated to just one megamolecule of proportionately larger mass. The megamolecules were treated as single Lennard-Jones centers, with the energy and distance parameters for each subgroup taken from the literature [20,29,30]. Such coarse-grained models have been used recently [39] to significantly reduce the computational burden associated with an all-atom approach.

For the actual simulation, a total of 128 DPPC chains (arranged on a uniform 8×8 square grid) and 3655 water molecules were used, yielding a ratio of 28:56:1 between water and the lipids. The total simulation volume was taken to a $6.8 \times 6.8 \times 6.8$-nm cubic box. The lipid bilayer was taken to have an initial thickness of 4.5 nm. Due to our use of a constant pressure coupling, the initial size is not critical since the system continually adjusts to match the external pressure. In all cases, before starting the field-dependent calculations of interest, this system was allowed to reach its self-consistent energy minimized state by running the MD simulations at zero electric field for 100 ps.

In order to facilitate meaningful comparisons with actual experimental results, two important aspects have to be considered. First, the microscopic electric field across an actual membrane has to be determined from a known averaged value representing the global voltage applied across the entire sample. Typically, such electric-pulse experiments are carried out by placing a buffered mixture containing the cells in a cuvette, as discussed in detail elsewhere [5,6]. Thus only the spatially averaged electric field is known from the applied voltage input and the physical separation between electrodes. The task of determining the microscopic membrane voltage from the global value was carried out here by a distributed circuit model, discussed in the next section. A second important point is that the microscopic membrane field is time dependent and hence the temporal details need to be included within the MD simulations. This was again carried out through the distributed circuit model (DCM). The DCM yielded a dynamic transmembrane voltage, which was discretized in a steplike fashion, and used as an input to the MD code.

B. Distributed circuit calculations

An approach to calculating the transmembrane potential is through a time-domain nodal analysis involving a distributed equivalent circuit representation of a cell and its membrane structures. The dynamic membrane electric field can then be obtained from the time-dependent transmembrane voltage. Details of this method and its implementation have been given elsewhere [40,41], and hence only a brief outline will be discussed here. Essentially, the entire cell volume was broken up into finite segments, and each segment represented by a parallel RC combination to account for the current flow and charging effects. Azimuthal symmetry was used to discard the φ co-ordinate (measured in a plane perpendicular to the applied electric field), while retaining only the radial (r) and angular (θ) coordinates of a spherical system. The computational region was a sphere that included the cell, its substructure, and surrounding suspension medium, discretized along the r and direction as shown in Fig. 2. For simplicity, membranes were taken as an integral unit, i.e., this subregion was not further discretized. For interior nodes, the current continuity equation is of the form

$$\sum_{k=1}^{6}\left(\sigma E + \epsilon\frac{\partial E}{\partial t}\right)_k \times A_k = \sum_{k=1}^{6} I_k = 0, \tag{1}$$

where I_5 and I_6 are currents along the ϕ direction, A_k is the surface area, E the electric field, ϵ the permittivity, and σ is the conductivity. Considerations of geometric symmetry of the computation region leads to $I_5 = I_6 = 0$ due to the equipo-

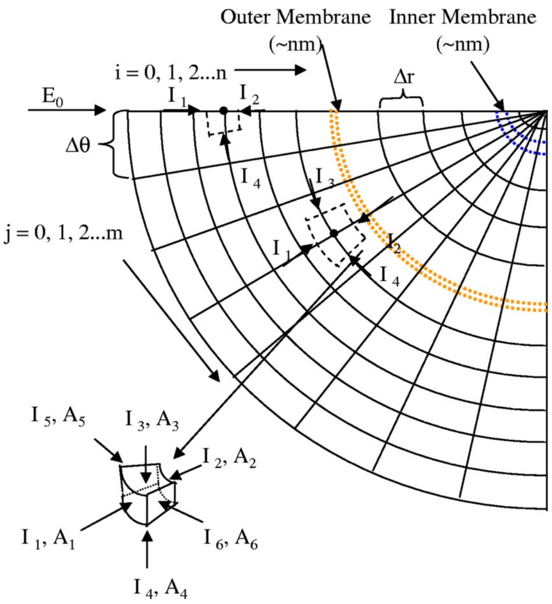

FIG. 2. (Color online) Schematic of one quarter of the model used to represent a cell for the distributed electrical calculations. The dotted box shows a typical element with current flows.

tentials. In order to reduce the computation load, only a quarter of the entire spherical computational region was considered based on the inherent symmetry. Nodes with $j=0$ and $j=m$ had to be treated carefully. Only I_1, I_2, and I_4 are nonzero since the targeted element only has five faces as face 3 shrinks to a line. For $j=0$ and $0<i<n$, Eq. (1) effectively becomes

$$
\begin{aligned}
&\sigma_1 \frac{V^t_{i-1,j}-V^t_{i,j}}{\Delta r}\left(r+\frac{\Delta r}{2}\right)^2\left[\cos\theta-\cos\left(\theta+\frac{\Delta\theta}{2}\right)\right]\\
&\quad+\sigma_2\frac{V^t_{i+1,j}-V^t_{i,j}}{\Delta r}\left(r-\frac{\Delta r}{2}\right)^2\left[\cos\theta-\cos\left(\theta+\frac{\Delta\theta}{2}\right)\right]\\
&\quad+\sigma_4\frac{V^t_{i,j+1}-V^t_{i,j}}{r\Delta\theta}(r\Delta r)\sin\left(\theta+\frac{\Delta\theta}{2}\right)+\frac{\epsilon_1}{\Delta t}\left(\frac{V^{t+1}_{i-1,j}-V^{t+1}_{i,j}}{\Delta r}\right.\\
&\quad\left.-\frac{V^t_{i-1,j}-V^t_{i,j}}{\Delta r}\right)\left(r+\frac{\Delta r}{2}\right)^2\left[-1-\cos\left(\theta+\frac{\Delta\theta}{2}\right)\right]\\
&\quad+\frac{\epsilon_2}{\Delta t}\left(\frac{V^{t+1}_{i+1,j}-V^{t+1}_{i,j}}{\Delta r}-\frac{V^t_{i+1,j}-V^t_{i,j}}{\Delta r}\right)\left(r-\frac{\Delta r}{2}\right)^2\left[-1\right.\\
&\quad\left.-\cos\left(\theta+\frac{\Delta\theta}{2}\right)\right]+\frac{\epsilon_4}{\Delta t}\left(\frac{V^{t+1}_{i,j+1}-V^{t+1}_{i,j}}{r\Delta\theta}-\frac{V^t_{i,j+1}-V^t_{i,j}}{r\Delta\theta}\right)\\
&\quad\times r\Delta r\sin(\theta+\Delta\theta/2)=0. \qquad (2)
\end{aligned}
$$

In the above, $\theta=\pi+j\times\Delta\theta=\pi$ and $\Delta\theta$ is $(\pi/2)/m$. For an electric field applied along the z direction (as shown in Fig. 2) and potential at node with $i=n$ is zero. Nodes with index $j=0$ are equipotentials, so $V_{i,m}=V_{n,j}=0$. Another boundary condition to be considered is for nodes with $i=0$. The potentials of such nodes is calculated as: $V_{0,j}=-E_0R\cos\theta$, for $j=0\cdots m$, where E_0 is the externally applied electrical field, and R the radius of the computational region.

TABLE I. Parameters used for the simulation.

Conductivities (S/m):	
Environment	0.6
Cell membrane	5.3×10^{-6}
Cytoplasm	0.13
Nuclear envelope	4.3×10^{-3}
Nucloplasm	0.18
Dielectric constant:	
Environment	80.0
Cell membrane	7.0
Cytoplasm	60.0
Nuclear envelope	22.8
Nucleoplasm	120.0
Geometry parameters:	
Radius of the simulation region	10 μm
Radius of cell	5.12 μm
Thickness of cell membrane	7 nm
Radius of nucleus	4.4 μm
Thickness of nucleus envelop	40 nm

Combining with the boundary conditions discussed above, one gets N equations for the N unknown node voltages. These N equations can easily be solved by any linear equation solver. Potentials on each node are easily updated at every time step based on the value of the externally applied field. In general, the membrane conductance is dynamic and depends on possible electroporation effects. This aspect had been taken into account by allowing for pore growth based on the Smoluchowski equation [40–42].

III. RESULTS AND DISCUSSION

Our distributed current model can predict the transmembrane electrical field, and was applied to the human Jurkat T lymphocyte cell. The parameters used in our study were measured in our laboratory, and are given in Table I. An experimental technique based on time domain dielectric spectroscopy (TDDS) as originally proposed by Feldman *et al.* [43] was used for our measurements. Details of the technique, and our application towards parameter extraction for various cell types are reported elsewhere [44]. The conductivity shown is for an intact membrane, and becomes time dependent upon pore formation and temporal evolution [40]. In our finite-difference implementation of the distributed circuit simulations, the grid spacing r was chosen to be 100 nm outside the membranes, and equal to their thickness at the membranes. The time step t was 0.01 ps. The time step was chosen to be well below the lowest internal time constant of the system.

Simulation results of the time dependent transmembrane potential for a cell subjected to a trapezoidal pulse are given in Fig. 3. The pulse was 0.01 V/nm in magnitude, with rise and fall times of 1.5 and 1.5 ns, respectively, and a 10-ns ON time. Such pulses are actually used in our laboratory quite

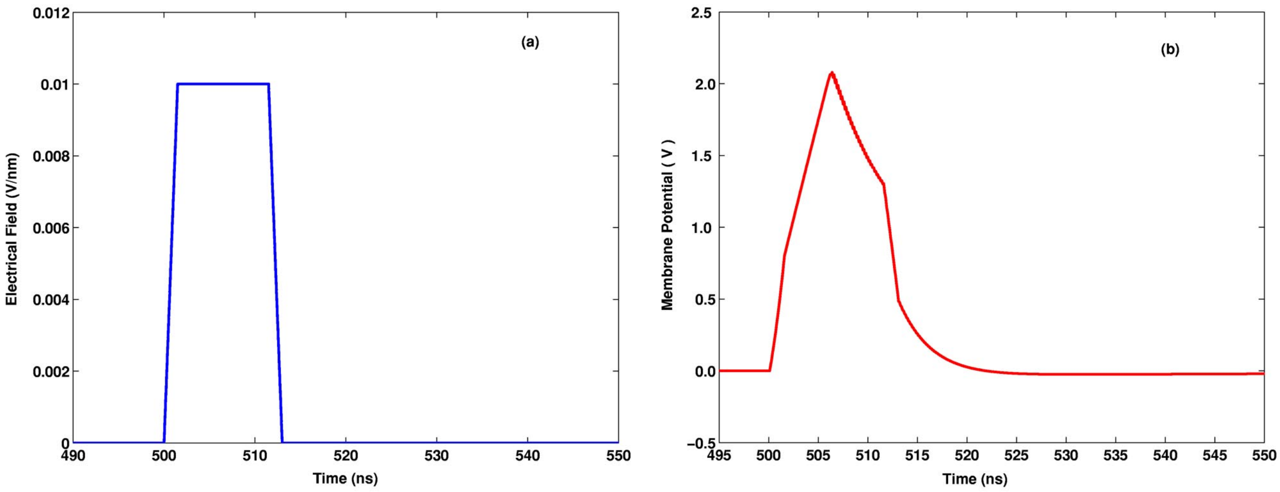

FIG. 3. (Color online) (a) External average applied electric field of 0.01 V/nm with a 10-ns duration, a 1.5-ns rise time, and 1.5-ns fall time. (b) Plasma transmembrane voltage versus time with input of (a).

routinely [5,6]. During the initial 500 ns of the simulation (as shown in Fig. 3), no external pulse was applied. This was done to allow the system to reach an initial steady state with an equilibrium distribution of nanopores within the membranes. In Fig. 3, the plasma membrane is predicted to porate within about 5–6 ns after the application of the pulse, leading to transmembrane voltage decay beyond these times. This numerical result appears to agree very well with recent experiments conducted in our laboratory. The measurements were based on time-dependent, field-induced shifts in luminescent intensity (at a fixed wavelength) from fluorescent dyes. Experimental details will be discussed elsewhere. Figure 3 also shows that a transient transmembrane overshoot beyond the conventional 1.0-V value for electroporation can occur under such transient, highly nonequilibrium conditions. The corresponding time-dependent electric field across the plasma membrane obtained from these DCM results was used as input into MD simulations to account for a realistic, time-dependent electric field. This approach effectively connected our macroscopic, distributed circuit model to the MD scheme, allowing for accurate study of membrane breakdown by a large external voltage.

As regards the MD study, a fundamental, first principles might arguably need to start with a set of randomly oriented lipids in the presence of a large number of water molecules. Upon running the MD simulations under energy minimization conditions for a very long time, a near-ordered lipid bilayer structure would emerge. In this configuration, the hydrophobic tails would expel the water molecules. However, this entire first-principles process would take a very long time. So instead, we adopt a slightly different approach by starting with an equilibrium stable system containing 128 DPPC lipids and 3655 water molecules as proposed by Tieleman *et al.* [36], and transforming it into our coarse-grain model. For simplicity and purposes of validation, our MD simulations were first carried out at zero electric field. Part of the objective was to compare the current course-grained model with an all-atom approach. Under these zero field conditions, one does not expect water molecules to penetrate the membrane. This is validated and clearly seen from our MD result for the spatial electron density distribution shown in Fig. 4. Electron density curves within DPPC and the water molecules have been shown for both the course-grained and an all-atom implementation. The absence of electron density over the central portion of the membrane is indicative of the inability of water molecules to pass through the membrane. These results are also very similar to a recent published report [42]. The close agreement helps validate the present model and its implementation.

Next, the effect of a realistic high-intensity, ultrashort electric field pulse was studied. After performing an energy minimization on this course-grained system, the electrical field obtained from Fig. 3 was applied. Snapshots showing the process of membrane configurational change are given in Fig. 5. Figure 5(a) shows the membrane to be well aligned (designated as the $t=0$ ns instant) right after the energy minimization was performed. After about 4.8 ns, some structural rearrangement (i.e., defect formation) begins to form at the

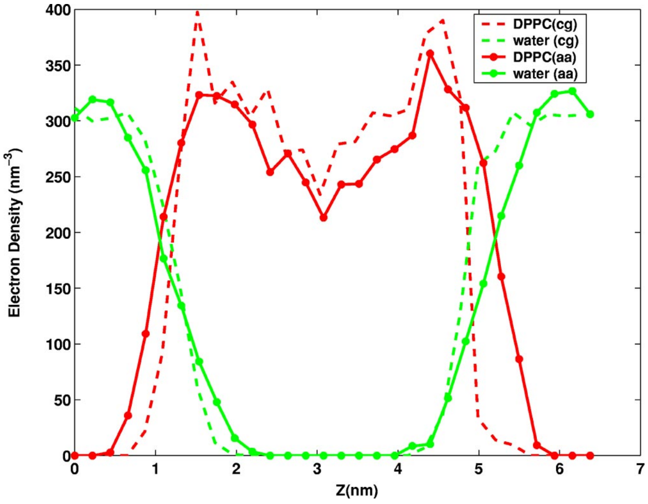

FIG. 4. (Color online) The spatial electron distribution for the coarse-grain (cg) model and all atom (aa) model.

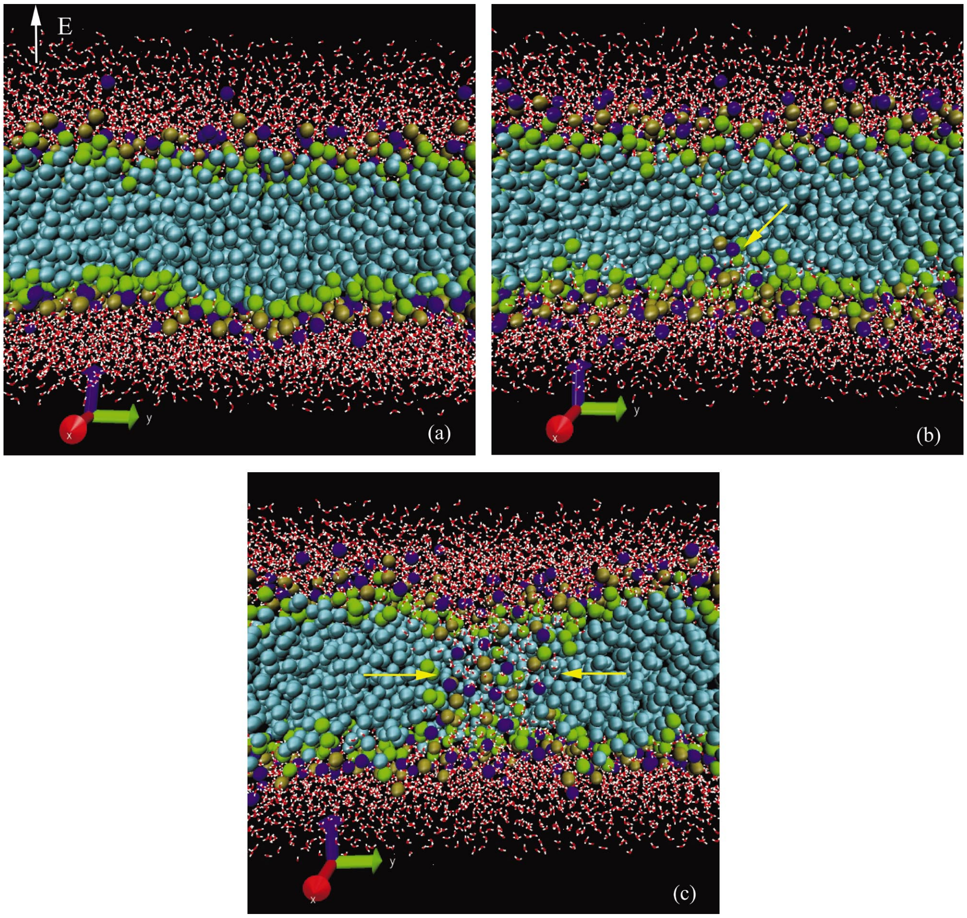

FIG. 5. (Color) MD snapshots of the electroporation process in a DPPC membrane under the *E* field of Fig. 3. (a) Initial configuration at $t=0$ ns; (b) structural rearrangement begins at the membrane bottom (anode side) at about $t=4.8$ ns; (c) a pore predicted to form at $t=5.3$ ns.

anode side (i.e., the membrane bottom) as shown in Fig. 5(b). A pore is then seen to form fairly quickly after the creation of the initial defect. In fact, a complete nanopore formation is predicted within about 0.5 ns after the initial structural change. Obviously, most of the time for the electroporation process is taken up by the initial defect formation. A pore, formed at 5.3 ns, is shown in Fig. 5(c).

This result demonstrates several important points. First, there is a very good match between the MD result of Fig. 5, predictions of our distributed current model, and actual experimental data [45]. In all cases, a nanopore is predicted to occur within about 5–6 ns at these high field intensities applied to the cells. Since the pulse duration is typically longer than this time, ion transport (especially for ions with smaller radii) would be very likely. Second, the initial structural rearrangement and dipole reorientation is a critical step in the electroporation process. Once such an initial breakthrough is achieved, the poration process proceeds relatively quickly. Finally, the poration process has a polarity dependence, and begins on the anodic side of a membrane. The related physics can easily be understood by considering the dipolar configuration within the DPPC membrane. Figure 6 shows a simple schematic of the membrane lipids with their dipoles located at the head groups. For each DPPC chain, the head group contains a dipole with positive charge on choline and the negative charge centered on the phosphate group. Initially, with no electric field present, the dipoles are in random thermal motion with the positive charges residing on the outermost portions of the lipid. Electrical field induced defects are initiated by the movement of dipoles on the surface of the membrane. Defects start to form on the anode side of the membrane because positively charged molecules (e.g., choline) on this side are forced to swing around (i.e., reorient in the presence of a strong external electric field) and enter the membrane. However, this same applied electrical field, when acting on the dipoles located at the cathodic membrane surface, merely works to stretch the dipoles without any molecular movement into the membrane volume. Thus Fig. 6(a) shows randomly distributed dipoles at the head groups on either side of the membrane as the initial configuration. Fig-

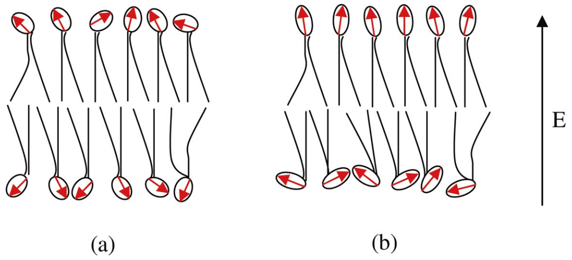

FIG. 6. (Color online) Schematic of the pore initiation process at the DPPC membrane. The arrows represent dipoles on the head groups of lipid molecules. (a) Initial configuration without an externally applied field, and (b) the configuration and expected movement of the dipole head groups upon the application of an external electric field.

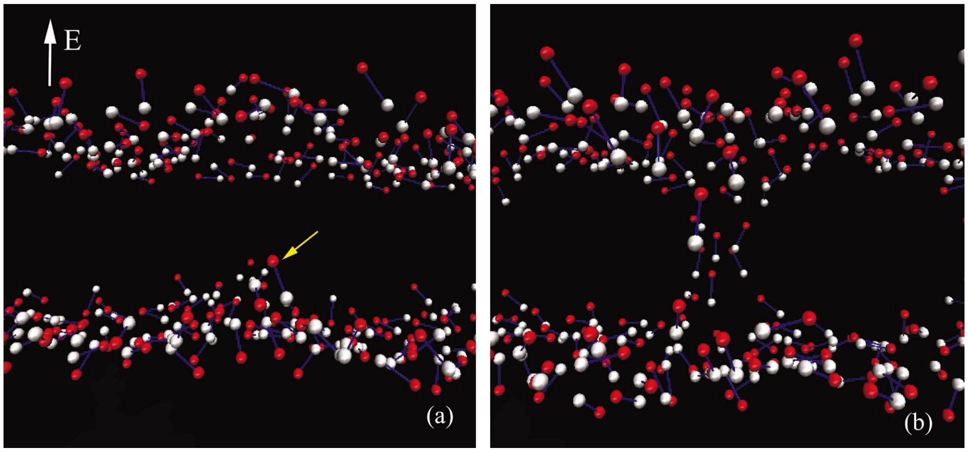

FIG. 7. (Color) Head-group dipoles of DPPC membrane for a fixed 0.5 V/nm field. Choline is in red, and phosphate in white. (a) ~2.65-ns snapshot showing the anodic-side defect, and (b) the ~3.3-ns snapshot at the initiation of the membrane pore.

ure 6(b) shows the alignment of dipolar head groups on the anodic side gradually deviating from the normal (equilibrium) orientation, and a defect starting to form. A similar process is actually seen to occur during the course of the MD simulations as shown in Fig. 7. The results shown in Fig. 7 are identical to the variable field case discussed in Fig. 5, but different times and spatial views have been chosen for clarity. Starting from an initially intact membrane structure, a defect is seen to initiate at the anodic side in Fig. 7(a) as indicated by the arrow. Finally, the entire pore forms in Fig. 7(b) as the hydrophilic head groups reorient to form a semicircular lining.

In addition to the variable electric-field case shown in Fig. 5, a separate simulation was also carried out for a fixed field of 0.5 V/nm. Choosing a constant electric field was aimed at bringing out the difference in pore formation times with respect to the variable voltage case, and also to facilitate a rough comparison with a recently published data by Tieleman's group [36] where an all-atom model was used. Figure 8(a) shows the top view of the final membrane configuration obtained from MD simulations after about 3.3 ns at the constant field of 0.5 V/nm. The cross-sectional view appears in Fig. 8(b), and clearly shows the head groups lining the pore. The pore is predicted to be about 1.5 nm in diameter, and somewhat narrower at the central point. This pore formation time was close to the result reported by Tieleman *et al.* [36], and faster than that for the variable electric field case of Fig. 5.

Finally, we probe the role of ions in the pore formation process. The electrostatic force on ions under such high-intensity electrical fields is in the range of $\sim 10^{-10}$ N. As a result, one can expect a continuous bombardment of the membrane surface by ions. This would certainly introduce additional Coulombic forces on the dipolar head groups with a nonlinear dependence on ionic proximity. This additional force would contribute to dipolar deflection and aid the defect formation process. This aspect was probed by randomly including 20 Na^+ and 20 Cl^- ions in the aqueous regions of the MD simulation volume. Charge neutrality was thus maintained within the entire system. Prior to running the MD calculations on the DPPC membrane system, however, test cases in bulk water were simulated to validate and cross check the predicted ionic mobilities. The numerical tests yielded diffusion coefficients of about $\sim 2.11 \times 10^{-9}$ m^2/s for Cl^-, around $\sim 1.21 \times 10^{-9}$ m^2/s for Na^+, and roughly $\sim 0.85 \times 10^{-9}$ m^2/s for Ca^{2+}. These values are roughly in keeping with the values reported previously [46]. In the case of Na^+ and Cl^- ions, one might expect Cl^- to have a slightly stronger affect due to the attractive force between Cl^- and the positive charged choline atoms within the lipid head groups. Practically however, cations are easier to detect in experiments.

Figure 9 shows snapshots of the electroporation process of a DPPC membrane with Cl^- and Na^+ in the aqueous environment under the time-dependent electric field of Fig. 3. In Fig. 9, the Cl^- ions are in yellow, while the Na^+ ions are

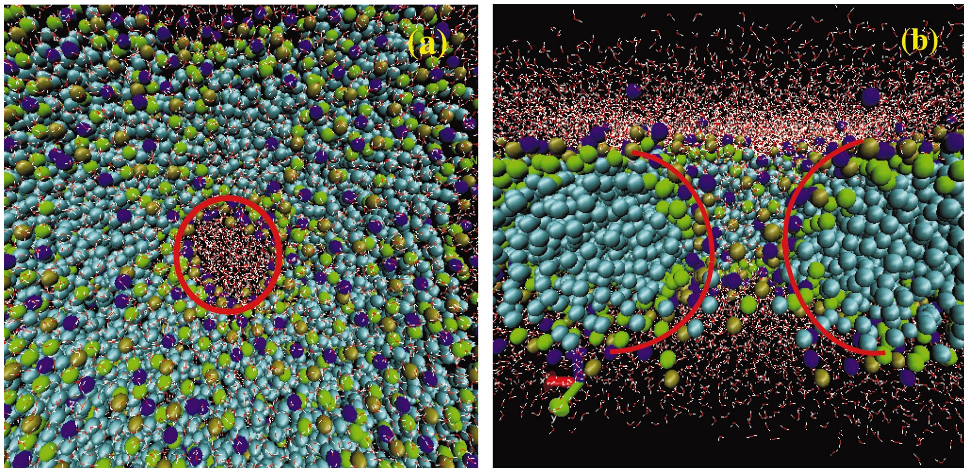

FIG. 8. (Color) MD based pore formation results for a fixed 0.5 V/nm field. The pore is about 1.75 nm in diameter at the widest part. (a) Top view of the membrane, and (b) a view of the cross-sectional slice.

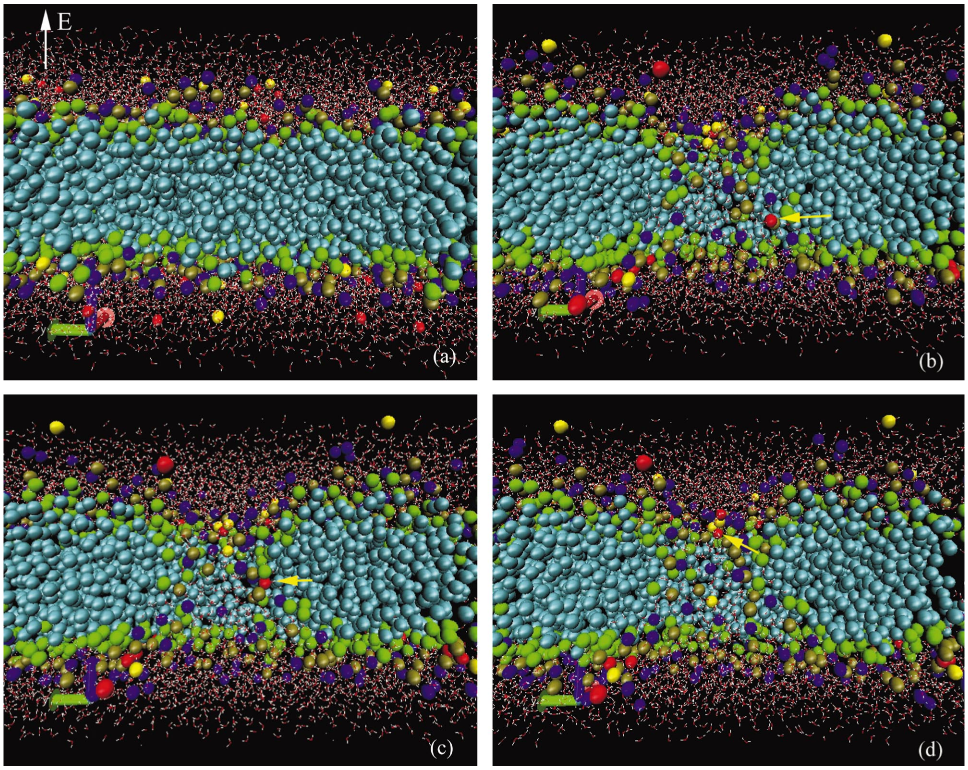

FIG. 9. (Color) Snapshots of the electroporation process of a DPPC membrane in the presence of Cl^- and Na^+ ions in the water. Cl^- is in yellow and Na^+ is in red. (a) Initial configuration when $t=0$ ns; (b) a pore forms and Na^+ starts to go in at $t=4.4$ ns; (c) Na^+ in the middle of the pore at ~5.02 ns; (d) Na^+ about to leave the pore at ~5.4 ns.

shown in red. The circled sodium ion was traced, and is clearly seen to pass through the membrane via an aqueous pathway that formed after about 4.4 ns. The snapshots at various times of 0, 4.4, 5.02, and 5.4 ns are shown in Figs. 9(a)–9(d). The sodium ion is seen to move up into the membrane at about 4.4 ns [Fig. 9(b)]. It appears near the middle of the pore after roughly 5.02 ns, and finally emerges at the opposite end at about 5.4 ns [Fig. 9(d)]. No sodium ion was found to go directly through the membrane before the poration process. These results clearly demonstrate that the occurrence of pores can be hastened and facilitated by the presence of ions presented in the system. In practical systems, however, the density of ions would be much lower. Consequently, the role of ions would be negligible, expecting for special structures (e.g., the endoplasmic reticulum) containing a high density of divalent Ca^{2+} ions. Poration and the subsequent release of Ca^{2+} upon the application of large external electric fields in such membranes appear to be plausible.

IV. SUMMARY AND CONCLUSIONS

A combined MD simulation scheme and a distributed circuit model were used for self-consistent predictions of the membrane response of a cell subjected to an ultrashort and high-intensity external electric pulse. In keeping with actual experiments, the average value of the applied electric field was taken to be 0.01 V/nm. The primary goal was to develop the computational capability of treating the dynamical aspects at the molecular level, without resorting to a full-blown, all-atom molecular dynamics. In addition, a variable electric field was included into the MD simulations for realistic and accurate response predictions. A coarse-grain model was used to incorporate most of the underlying physics for analysis of the observed biological phenomena. Instead of applying the full and complete atomic details, this approach resorted to the inclusion of only the essential kinetic and stochastic features inherent in the system. Thus, for example, the DPPC lipid molecules were simply represented by a 12-ball model. Essential features such as the hydrophilic and hydrophobic nature of the lipid chain interactions were effective included, as were the clustering of water molecules around ions due to the electric field gradients at the microscopic level, and the detailed intermolecular force functions.

The numerical simulation scheme allowed the inclusion of the stochastic, kinetic nature of the molecular motion, and provided a complete dynamical picture with many-body screening. The time dependent details of pore formation at membranes in response to a variable electric field were probed, and this variable membrane field was computed from a distributed current model applied to the entire cell. Our results showed that nanosized pores could typically be formed for spatially averaged external fields on the order of 0.01 V/nm. The formation times were roughly on the order of 5–6 ns, with a decreasing delay at higher fields. The predictions were in very good agreement with recent experimental data on Jurkat cells. It was shown that defect formation on membranes would begin at sites located on the anode side. This polarity dependence resulted from the dipole charge distribution across the DPPC membrane.

The simulations suggest that field-induced pore creation can be aided by the presence of ions in medium surrounding the membrane. Divalent ions such as Ca^{2+} contained in the endoplasmic reticulum could be especially important. This would be the combined result of ionic bombardment, inclusion of Coulombic forces, and the spatial nonuniformity created within the local field distribution. An inhomogeneous field is most effective for facilitating interactions with dipolar molecules. Finally, these results suggest that other transport events such as the observed phosphatidylserine (PS) externalization can be triggered by such pulses with duration on the order of ~10 ns. Though the details will be addressed in a subsequent contribution, the likely sequence would be an initial pore formation, followed by the diffusion of charged molecules around the defect.

ACKNOWLEDGMENTS

This work was sponsored in part by the Air Force Office of Scientific Research (Contract No. F49620-01-1-0506) on Bio-Inspired Concepts and AFOSR-MURI Grant (No. F49620-02-1-0320) on Subcellular Responses to Narrowband and Wideband Radio Frequency Radiation. The authors would also like to acknowledge useful discussions with J. Weaver (MIT), E. Neumann (University of Bielefeld), and D. P. Tieleman (University of Calgary).

---

[1] K. H. Schoenbach, S. J. Beebe, and E. S. Buescher, Bioelectromagnetics (N.Y.) **22**, 440 (2001).
[2] R. P. Joshi, Q. Hu, R. Aly, K. H. Schoenbach, and H. P. Hjalmarson, Phys. Rev. E **64**, 011913 (2001).
[3] K. H. Schoenbach, F. E. Peterkin, R. W. Alden, and S. J. Beebe, IEEE Trans. Plasma Sci. **25**, 284 (1997).
[4] H. Huelsheger, J. Potel, and E. G. Niemann, Radiat. Environ. Biophys. **20**, 53 (1981).
[5] S. J. Beebe, P. M. Fox, L. J. Rec, L. K. Willis, and K. H. Schoenbach, FASEB J. **17**, 1493 (2003).
[6] J. Deng, K. H. Schoenbach, E. S. Buescher, P. S. Hair, P. M. Fox, and S. J. Beebe, Biophys. J. **84**, 2709 (2003).
[7] P. T. Vernier, Y. Sun, L. Marcu, S. Salemi, C. M. Craft, and M. A. Gundersen, Biochem. Biophys. Res. Commun. **310**, 286 (2003).
[8] S. J. Beebe, P. M. Fox, L. J. Rec, K. Somers, R. H. Stark, and K. H. Schoenbach, IEEE Trans. Plasma Sci. **30**, 286 (2002).
[9] K. H. Schoenbach, R. P. Joshi, J. Kolb, N. Chen, M. Stacey, P. Blackmore, E. S. Buescher, and S. J. Beebe, Proc. IEEE (to be published).
[10] P. T. Vernier, Y. Sun, L. Marcu, C. M. Craft, and M. A. Gundersen, Biophys. J. **86**, 4040 (2004).
[11] S. J. Beebe, P. F. Blackmore, J. White, R. P. Joshi, and K. H. Schoenbach, Physiol. Meas **25**, 1077 (2004).
[12] S. J. Beebe, J. White, P. F. Blackmore, Y. Deng, K. Somers, and K. H. Schoenbach, DNA Cell Biol. **22**, 785 (2003).
[13] R. M. Venable, Y. Zhang, B. J. Hardy, and R. W. Pastor, Science **262**, 223 (1993).
[14] E. Egberts, S. Marrink, and H. J. C. Berendsen, Eur. Biophys. J. **22**, 423 (1993).
[15] T. R. Stouch, Mol. Simul. **10**, 335 (1993).
[16] H. Heller, M. Schaefer, and K. Schulten, J. Phys. Chem. **97**, 8343 (1993).
[17] J. J. L. Cascales, J. G. de la Torre, S. J. Marrink, and H. J. C. Berendsen, J. Chem. Phys. **104**, 2713 (1996).
[18] D. P. Tieleman and H. J. C. Berendsen, J. Chem. Phys. **105**, 4871 (1996).
[19] M. P. Allen and D. J. Tildesley, *Computer Simulations of Liquids* (Clarendon Press, Oxford, 1987).
[20] E. Egberts and H. J. C. Berendsen, J. Chem. Phys. **89**, 3718 (1988).
[21] W. F. van Gunsteren and H. J. C. Berendsen, Angew. Chem., Int. Ed. Engl. **29**, 992 (1990).
[22] H. J. C. Berendsen, J. P. M. Postma, W. F. Gunsteren, and J. Hermans (Reidel, Dordrecht, 1981).
[23] H. J. C. Berendsen, J. Grigera, and T. Straatsma, J. Phys. Chem. **91**, 6269 (1987).
[24] W. L. Jorgensen, J. Am. Chem. Soc. **103**, 335 (1981).
[25] R. Pastor and R. Venable, *Computer Simulation of Biomolecular Systems: Theoretical and Experimental Applications*, edited by W. van Gunsteren, P. Weiner, and A. Wilkinson (Escom Science, Leiden, 1993).
[26] H. J. C. Berendsen, J. P. M. Straatsma, W. F. van Gunsteren, A. DiNola, and J. R. Haak, J. Phys. Chem. **81**, 3684 (1984).
[27] L. Verlet, Phys. Rev. **159**, 98 (1967).
[28] R. W. Hockney and J. W. Eastwood (McGraw-Hill, New York, 1981).
[29] D. van der Spoel, A. R. van Buuren, E. Apol, P. J. Meulenhoff, D. P. Tieleman, A. L. Sijbers, R. van Drunen, and H. J. C. Berendsen, GROMACS User Manual, Version 1.2, 1996.
[30] H. J. C. Berendsen, D. van der Spoel, and R. van Drumen, Comput. Phys. Commun. **91**, 43 (1995).
[31] E. Lindahl, B. Hess, and D. van der Spoel, J. Mol. Model. **7**, 306 (2001).
[32] H. J. C. Berendsen, J. P. Postma, W. F. Gunsteren, and J. Hermans, in *Intermolecular Forces*, edited by B. Pullman (Reidel, Dordrecht, Amsterdam, 1981), pp. 331–342.
[33] D. Tieleman, S. J. Marrink, and H. J. C. Berendsen, Biochim. Biophys. Acta **1331**, 235 (1997).
[34] J. Nagle, R. Zhang, S. Tristram-Nagle, W. Sun, H. I. Petrache, and R. M. Suter, Biophys. J. **70**, 1419 (1996).
[35] J. Nagle and S. Tristram-Nagle, Biochim. Biophys. Acta **1469**, 159 (2000).
[36] D. P. Tieleman, H. Leontiadou, A. E. Mark, and S. J. Marrink, Comput. Phys. Commun. **125**, 6382 (2003).
[37] W. F. van Gunsteren and H. J. C. Berendsen, Mol. Phys. **34**, 1131 (1977).
[38] J. P. Ryckaert, G. Ciccotti, and H. J. C. Berendsen, J. Comput. Phys. **25**, 327 (1977).
[39] C. F. Lopez, P. B. Moore, J. C. Shelley, M. Y. Shelley, and M. L. Klein, Comput. Phys. Commun. **147**, 1 (2002).
[40] R. P. Joshi, Q. Hu, K. H. Schoenbach, and S. J. Beebe, Phys. Rev. E **69**, 051901 (2004).
[41] R. P. Joshi, Q. Hu, and K. H. Schoenbach, IEEE Trans. Plasma Sci. **32**, 1677 (2004).
[42] R. P. Joshi, Q. Hu, K. H. Schoenbach, and H. P. Hjalmarson, Phys. Rev. E **65**, 041920 (2002).
[43] I. E. Yu. Feldman and Y. Hayashi, IEEE Trans. Dielectr. Electr. Insul. **10**, 728 (2003).
[44] A. L. Garner, N. Chen, J. Yang, J. Kolb, R. J. Swanson, K. C. Loftin, S. J. Beebe, R. P. Joshi, and K. H. Schoenbach, IEEE Trans. Plasma Sci. **32**, 2073 (2004).
[45] J. Kolb (private communication).
[46] S. Edwards, B. Corry, S. Kuyucak, and S. Chung, Biophys. J. **83**, 1348 (2002).